Interior insulation – Experimental investigation of hygrothermal conditions and damage evaluation of solid masonry façades in a listed building

Odgaard, Tommy; Bjarløv, Søren Peter; Rode, Carsten

Published in:
Building and Environment

Link to article, DOI:
10.1016/j.buildenv.2017.11.015

Publication date:
2018

Document Version
Peer reviewed version

Interior insulation – Experimental investigation of hygrothermal conditions and damage evaluation of solid masonry façades in a listed building

Tommy Odgaard[a,b,*] , Søren Peter Bjarløv[a], Carsten Rode[a]

[a] Technical University of Denmark, Department of Civil Engineering, Brovej 118, 2800 Kongens Lyngby, Denmark. SPB@byg.dtu.dk & CAR@byg.dtu.dk.

[b] COWI A/S, Parallelvej 2, 2800 Kongens Lyngby, Denmark. TOOG@COWI.dk.

[*] Corresponding author. E-mail: TOOG@COWI.dk, Postal address: Parallelvej 2, 2800 Kongens Lyngby, Denmark.

Abstract

Exterior walls in historic multi-storey buildings compared to walls in modern buildings have low thermal resistance, resulting in high energy loss and cold surfaces/floors in cold climates. When restrictions regarding alteration of the exterior appearance exist, interior insulation might be the only possibility to increase occupant comfort.

This paper describes an investigation of the hygrothermal influence when applying 100 mm of diffusion open interior insulation to a historic multi-storey solid masonry spandrel. The dormitory room with the insulated spandrel had a normal indoor climate with a maximum observed monthly average humidity by volume excess of 3.2 g/m³ during the experiment.

Relative humidity and temperature were monitored manually using wooden dowels over 2 years and 8 months in two solid masonry spandrels: one insulated wall and one untreated wall. The investigation showed that installing insulation on a solid masonry spandrel induced hygrothermal changes: Uniformly distributed higher relative humidity and lower temperature throughout the masonry, compared to an un-insulated wall. The relative humidity of the un-insulated masonry wall was in the range 50 % on the inside to 60 % on the outside, while the insulated wall showed uniformly distributed values around 80 %.

The risk of moisture-induced damage was evaluated based on mathematical models for mould and decay of wood, visual inspection for frost and mould, and on-site measurements for presence of mould spores. The damage evaluation showed no risk of damage from the changed hygrothermal conditions when applying interior insulation to a solid masonry spandrel.

Keywords: historical; masonry; insulation; moisture; damage; experimental

1 Introduction

With today's focus on reducing heat loss, Danish multi-storey buildings with solid masonry walls receive increasing attention due to their large potential for reducing heat loss and consequent reduction of CO_2 emissions [1,2]. The overall heat loss can be simplified to a vertical component through roof and ground, and a horizontal component through the façade, including the gables when exposed. Research shows that considerable energy savings can be achieved by applying thermal insulation to the solid masonry walls of

historic multi-storey buildings [3,4]. The spandrels underneath the windows are the thinnest walls in traditional multi-story buildings and are responsible for a considerable part in the overall heat loss of the facade. The walls are characteristically 1-stone thick (238 mm), and have an interior layer of plaster [5,6]. 1-D hygrothermal simulation in WUFI of an uninsulated spandrel showed a minimum temperature on the inside of 9.2 ^{0}C [7] when simulating with a Danish design year [8]. Occupants staying in rooms with cold surfaces can suffer from discomfort due to asymmetric radiation from surfaces when larger than 10 ^{0}C [9,10], cold floors [11,12] and draught. Occupant comfort will increase, when the exposure to cold surfaces are reduced.

From a building physics point of view, the best location for adding insulation to a solid masonry wall is on the exterior side [13–15]. However, from a building preservation point of view, exterior insulation is often not a possibility. E.g., preservation of the exterior appearance of listed and worth-to-preserve buildings is a mandatory requirement in Denmark. With worth-to-preserve buildings, interior insulation is therefore often the only possibility.

Previous research has focused on how to add interior insulation on old masonry structures and the performance of the insulation material [3,16–22]. Aiming for energy reduction and temperature increase of the thinnest parts of the façade, Odgaard et al. showed that for a multi-storey building with 2-stone (468 mm) wall columns with interior rendering, up to 40 % of the possible U-value reduction by applying interior insulation to the entire interior masonry wall, could be achieved by insulating the spandrels [23].

Hygrothermal conditions in the original solid masonry wall become worse when adding thermal insulation to the interior side. The heat flow from the room to the original wall will be reduced [24], possibly causing condensation to form behind vapour open insulation [15,25]. The moisture content increases in the original wall, and leads to high moisture content on the cold side of the newly added insulation material [15,22,24,26–29].

The changed hygrothermal conditions will increase the risk of damages. One being the risk of frost damage [15], governed by 3 criteria occurring at the same time [30]: Temperature below freezing; wet masonry; and material sensitivity to frost. Another being the risk of mould and decay of wood occurring, governed by [31]: temperature; relative humidity; exposure time; and material.

Mould risk can be assessed mathematically based on monitored relative humidity and temperature, or based on on-site measurements. A large amount of different mathematical mould models exist in literature. Comparison of models have previously been done in [32] for wood, whereas review of the models including other material surfaces were included in [33]. A transfer model that converts the "growth-in-mm" results from the bio-hygrothermal model of Sedlbauer [34,35], the model used in WUFI, to the mould index model developed by Ojanen et al. [36], the model used in Delphin were described in [37]. Mathematical mould risk evaluation in this paper was based on the model from VTT [36,38], with risk evaluation based on the defined limits for maximum allowed mould index values at the interior side and interstices in the structure [37]. Different approaches for on-site measurements exist [39–41]. As the aim of present investigation is to detect if mould growth occurs, and not to detect specific mould species, it was decided to use the Mycometer®-test method [42].

A review of different mathematical decay models were performed by Brischke and Thelandersson, with a focus on outdoor conditions. As the models were based on temperature, relative humidity and exposure time, the models must also be appropriate for wood performance in other positions where oxygen is available. A range of parameters, which should be included in an appropriate model for decay of wood, were described in [43]: The importance of wood type, the need for inclusion of lag/activation process and how dose-response functions are appropriate for the biological field. The model of H. Viitanen et al. [44] included the mentioned parameters, where the inclusion of the activation process, defined as an index "α", resulted in a dose-response function that comprises the lag effect. The model in [44] was based on Pine

Sapwood, the structural lumber in historic Danish Multi-storey buildings traditionally consist of Pomeranian Pinewood, both heartwood and sapwood [5,6]. Oxygen will be naturally present in the traditional floor constructions of historic multi-storey buildings, which consist of layers of open air and clay.

Hygrothermal conditions in the experiment were monitored using wooden dowels drilled into the walls of interest. The use of wooden dowels to monitor hygrothermal conditions in structures is well-known and has proven as a stable methodology for long-term measurements [45–47], with examples of sensors working for a minimum of 20 years [48]. The conversion of resistance and temperature measurements in wooden dowels to wood moisture content is described both in Danish [49–52] and international literature stating the applicability of wooden dowels for slow and long term-measurement of relative humidity [53,54].

The aim of this paper is to present the results of an investigation of changed hygrothermal conditions when applying interior insulation to a reduced part of the interior surface, specifically the spandrels of a historic solid masonry wall. This has been conducted experimentally by installing interior insulation in the old historic Borchs Dormitory from 1823, situated in the Danish capital, Copenhagen. The dormitory consists of solid masonry walls with a rendered and painted facade. The study focused on reduction of heat loss and improvement of the indoor climate without risk of damage by frost, mould or decay of wood. The hygrothermal conditions were monitored in two walls, one with and one without interior insulation. Døi and Nielsen started the monitoring period in November 2014 with 1½ months of measurements [55]. The hygrothermal conditions continued to be monitored as reported in the present study, and comprises a total monitoring period of 2 years and 8 months.

2 Method

2.1 Experimental setup - building composition

Borchs dormitory was built in year 1823 and is situated at the coordinates (55.6805°N, 12.5744°E). A picture of the façade and overview of the area can be seen in Figure 1. The buildings north and northwest of the garden/courtyard in front of the façade have a height of 4-5 stories + roof, which limits the influence from dominant western winds and wind driven rain. The exterior façade consists of solid masonry walls, constructed from historic red clay bricks and lime mortar, with no built in thermal insulation. The windows do not have an external sill. The position of the windows follow building tradition, situated approximately 4 cm from the exterior surface into the building, leaving 4 cm of masonry at the bottom, top and sides of the wall around the window exposed to rain. The infiltration of rainwater is reduced by a layer of rendering and paint covering the exterior side of the masonry wall. This rendering was originally performed with lime mortar, which might have been repaired with rendering systems with content of Portland cement at later stages. The masonry wall is also rendered and painted on the interior side. The building has four storeys, three of which have rendered and painted vertical facades and a 4th storey below the sloped roof. The façade in each of the North-West facing rooms on the floor above ground used for the experiment, Room 9 and 12, consists of two spandrels. One spandrel in each room has a radiator in front; the other spandrel is blank and is used for the experiment. The exterior surface of the spandrels used in the experiment was inspected from ground level and showed no visible cracks in the façade.

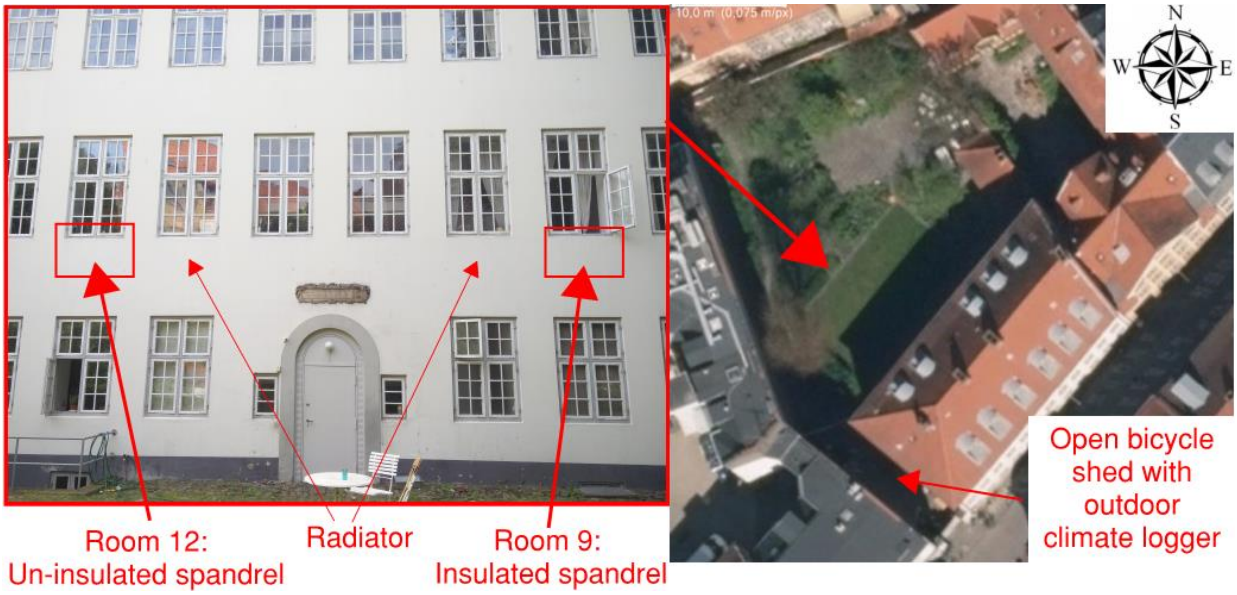

Figure 1 Picture of façade used in experiment. Overview courtesy of Maps from COWI.

The preservation class of the dormitory was at the time of investigation defined as “Listed” [56], a classification demanding for preservation of the interior and exterior expressions. A range of energy saving measures were discussed with representatives from the Danish Agency for Culture and Palaces in [55]. The only possible energy saving measure, which could be allowed by the Agency for Culture and Palaces, was internal insulation of an spandrel, where the limited extend of insulation coverage was defined by architectonic components on the inside surface. The material usage had to be limited to products with possibility for re-establishment at a later stage, a criterion that 100 mm of the diffusion open thermal insulation system "Ytong Multipor Mineral Insulation Boards" fulfilled. The manufacturer has provided the material characteristics: Density, ρ = ~115 kg/m³, thermal conductivity, λ = 0.045 W/(m·K), water vapour resistance factor, μ = 3 (light mortar ≤ 10). The insulation was installed by the manufacturer, following their normal specifications by fully bonding the insulation board to the original interior rendering and covering the interior side of the insulation board with the same light mortar.

The insulation system was installed on the inside of the blank spandrel in Room 9, while the blank spandrel in Room 12 was kept untreated, as seen in Figure 1. A detailed drawing of the insulated wall can be seen in Figure 2. The un-insulated wall was similar to the insulated wall, without the insulation system.

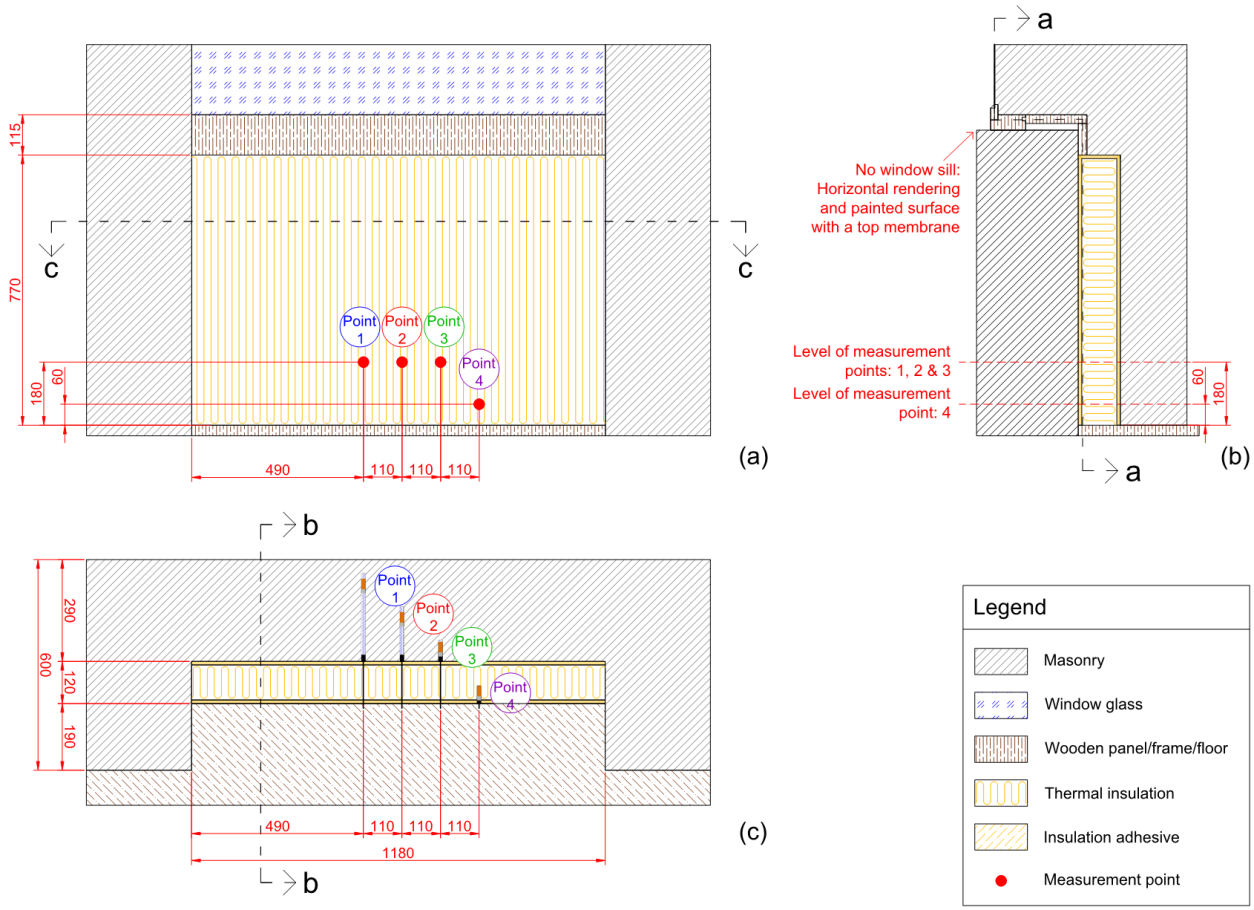

Figure 2 2-dimensional sketches of construction.

2.2 Indoor and outdoor humidity by volume [v]

The measured indoor conditions in both rooms were assessed, to determine if the monitored moisture conditions in the experiment were within normally expected values. The values were assessed according to the internal humidity classes in Appendix A.2 of [57] and Chapter 3.3.3 of [13], based on interpolated values from the indoor and outdoor temperature and relative humidity loggers. The interpolation ensured similar data steps for the comparison. The outdoor values were based on monthly average values from a locally placed logger, as can be seen in Figure 1. The average indoor excess of humidity by volume was found by subtracting the summarized monthly outdoor humidity by volume from the summarized indoor humidity by volume and dividing the result by the number of data points in the month. The vapour pressure and humidity by volume was determined mathematically by the empirical expressions from [57].

2.3 Measuring equipment

The conditions in the walls were monitored in three sensor points by manual readings. The measurement strategy was based on DC electrical resistance measurements in wooden dowels and thermal measurements in soldered copper and constantan wire, both measured with a T301.COW instrument [58,59]. A measurement period of 20 seconds [52] was used for the electrical resistance measurements, whereafter the value was noted. All wooden dowels were pushed as long as possible into drilled holes of various depths from the interior side, as illustrated in Figure 2 and Figure 3. All holes were closed with acrylic sealant on the surface of the interior masonry to hinder convective exchange of air between the air in the drilled hole and the inside environment. The sealant was applied from the top of the wires, reaching 1-2 cm into the holes with possible small voids along/underneath the wire. The wires and dowels were

placed loosely in the drilled holes without additional sealant around the wire and dowel. The depths of the drilled holes were defined in [55], and the locations of the wooden dowels were measured at the end of the experiment. Only sensors 1, 2 and 3 in the un-insulated wall and sensor 4 from the insulated wall were removed, as the insulation board was left in place. For the insulated case, the wires were run to the floorboards and into the room, where after the insulated board was installed, covering the drilled holes.

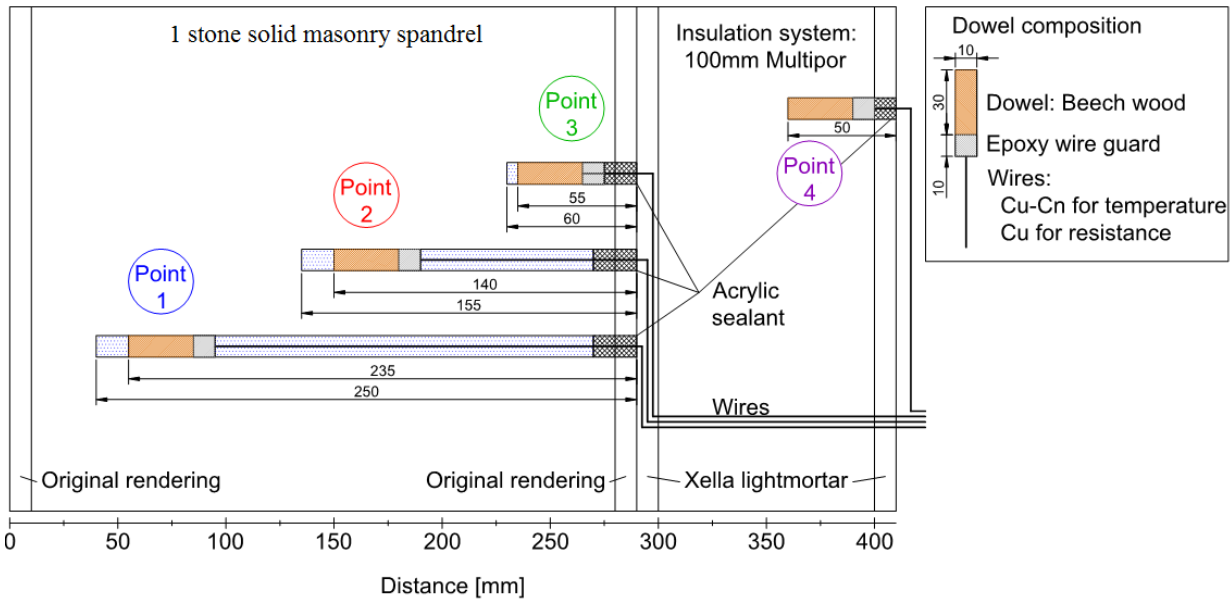

Figure 3 Illustration of dowel placement. Resistance is measured in the wooden dowel; temperature is measured in the epoxy wire guard. Blue = air, brown = wooden dowel. Colours of point numbers are consistent throughout the paper.

Monitoring of the hygrothermal conditions in the wall ran from November 2013 until July 2016. The insulation was installed in December 2013. The resistance and temperature measurements of the wooden dowels were performed with the following intensity: 2013-11-25 → 2014-01-23 every ~3-5 days; → 2014-06-04 every ~14 days; → 2016-07-15 every ~1-2 months.

The indoor and outdoor climates were monitored by three Onset HOBO U12-012 temperature and relative humidity data loggers [60]. The loggers were placed as illustrated in Figure 1, inside in Room 9 & 12 and outside in a nearby open bicycle shed. The conditions were monitored at minimum every 15 minutes in the entire monitoring period. The outdoor climate was further monitored by 2 nearby weather stations [61]. A station situated in Kastrup (Copenhagen Airport), 9 km south-southeast from Borchs dormitory, and a station situated in Jægersborg, 10 km north-northwest from Borchs dormitory. Running averages of the measured indoor and outdoor relative humidity and temperature boundary conditions were calculated with different time spans for the running average to better illustrate the values in graphs. The running averages were calculated as averages of the boundary condition values 0.5 x time span back and 0.5 x time span ahead of time for each data point.

2.3.1 Conversion, measured wooden resistance [*R*] to relative humidity [*RH*]

The calculation from DC electrical resistance to wooden moisture content by weight is based on [50], illustrated in equations (1) and (2). The equations fit with the graph for conversion of resistance to wooden moisture content by weight supplied with the dowels [62].

$$R_{adjusted}\ [log10M\Omega] = R\ [log10M\Omega] - (0.029 + 0.005 \cdot R\ [log10M\Omega]) \cdot (20 - \theta\ [^{o}C])\ \ [50] \qquad (1)$$

$$u\left[\frac{kg}{kg}\right] = 10^{\wedge}\left(\frac{12.63 - R_{adjusted}\,[log10M\Omega]}{9.196}\right) \text{ [50]} \tag{2}$$

Where: R = measured DC electrical resistance $[log10M\Omega]$, $R_{adjusted}$ = electrical resistance adjusted to 20 °C $[log10M\Omega]$, u = wooden moisture weight percent $\left[\frac{kg}{kg}\right]$.

Equation 3 is used to transform wooden moisture into relative humidity by curve fitting to the sorption isotherm for 750 kg/m³ beech wood in [63,64]. The relative humidity was determined as the mean result from the adsorption and desorption curves.

$$\mathrm{RH}(u)\,[\%] = 0.5 \cdot \left(\begin{array}{c} \left(C_{adsorption} \cdot \exp\left(1 - \left(\frac{u\left[\frac{kg}{kg}\right]}{A_{adsorption}}\right)^{B_{adsorption}}\right)\right) + \\ \left(C_{desorption} \cdot \exp\left(1 - \left(\frac{u\left[\frac{kg}{kg}\right]}{A_{desorption}}\right)^{B_{desorption}}\right)\right) \end{array} \right) \tag{3}$$

Where: RH = Relative humidity [%], *A*, *B* & *C* being the following factors for ad- and desorption: $A_{adsorption}$=7.608, $B_{adsorption}$=-1.353, $C_{adsorption}$=42.960, $A_{desorption}$=12.690, $B_{desorption}$=-0.8945, $C_{desorption}$=57.440.

2.4 Investigation of cold surfaces, wall and floor

An investigation of the thermal envelope of the dormitory building was performed in the start of the project in October 2013, before installation of interior insulation. The investigation was performed by a professional company, ISOLINK [65] with focus on detection of thermal irregularities of interior building envelope via infrared/thermographic pictures [66].

2.5 Mathematical model for calculation of mould risk [*M*]

It has been decided to base the mathematical mould evaluation in the present paper on the method developed by the Technical Research centre of Finland (VTT), and by Tampere University of Technology, Finland for wood based materials [38], later extended to evaluate other material types [36].

The mould index, abbreviated "*M*", is calculated based on a dataset with 60 min interpolated values of the original measurements. The mould index is defined as a value in the range 0 → 6, with each integer defining as a state of the mould growth [38]. The following basic factors were defined for the analysed case:

- Surface quality (*SQ*) and wood species (*W*): Only non-wood materials were modelled, resulting in *SQ* = *W* = 0 [37].
- Material class: "Medium resistant", as the Multipor and adhesive material is defined as cement based/aerated concrete [36].

The combined temperature and relative humidity limit for mould growth when using a "very sensitive" and "sensitive" material were defined in [36] by a limit of 80 % RH with a curve in the temperature range $\theta = 0\,^{o}C \rightarrow 20\,^{o}C$ as illustrated with label "*sensitive" in Figure 4. For a medium resistant material, a limit of 85 % RH was defined [36], but only from 20°C and above. In order to cover the temperature range $\theta = 0\,^{o}C \rightarrow 20\,^{o}C$, we suggest a 3rd degree polynomial curve fit to the following defined points: (θ, RH) = (0, 100; 20, 85; 25, 85; 30, 85). This resulted in the following equation: $\mathrm{RH}(\theta) = -0.001 \cdot \theta^3 + 0.075 \cdot \theta^2 - 1.85 \cdot \theta + 100$. Points and resulting fit can be seen in Figure 4 with the label "*resistant". There will be no mould growth for temperatures below 0°C.

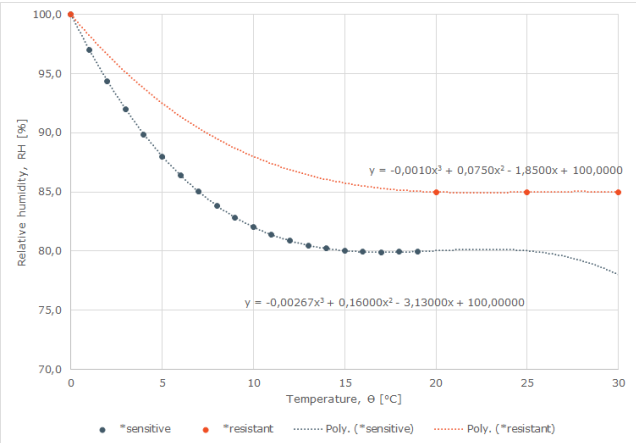

*Figure 4 Development of simple expression for mould limit of *resistant materials. *sensitive = limit from* [36].

Prediction of mould growth in boundary layers between materials were described in [36]. This work of Ojanen et al. further included the possibility for reduction of the mould index when the combined temperature and relative humidity conditions were outside the limit for mould growth, based on mould declination factors for a range of different materials. As a large spread existed in the declination factors for materials situated in the medium resistance category, the results in the present paper were modelled with the factor set to "almost no decline", "relatively low decline", and "significant relevant decline", being 0.1, 0.25 and 0.5 respectively [36].

The mould model was applied to two measurement points. Point 3 being the wooden dowel placed in the wall closest to the original interior surface, and Point 4 in the insulation board. The points are illustrated in Figure 2 and Figure 3.

2.6 Physical test for mould on-site via Mycometer®-test

Mould growth was tested on-site 1 year after termination of monitoring hygrothermal conditions. The investigations were performed on the interior surface, and in the interface between masonry and interior insulation. Mould growth was assessed using the method of Mycometer, with instructions by trained specialists at the consultancy firm COWI A/S and from the webpage of Mycometer [67,68].

The outcome of the test is FLouresence Units (*FLU*), a value that can be related to the N-acetylhexosaminidase activity found in mould. The magnitude of FLU defines a category interrelated to the presence of mould (spores), based on interpretation criteria set up by Mycometer [41,42,69].

The 3 categories of mould occurrence are [41,42,69]:

1. A: Below background level.
2. B: Above background level: "*... typically due to high concentrations of spores in dust deposits."* [69], "*… likely depositied fungal debris, which can often be found in older Mortar/Concrete materials."* [69].
3. C: High above background level: "*…due to mould growth…*" [69].

The performance of the Mycometer-test have been validated in relation to linearity and repeatability [70].

2.7 Model for calculation of irreversible mass loss by decay of wood [*ML*]

Evaluation of the risk for decay of wood is done with the extended mathematical model developed at the Technical Research centre of Finland (VTT) [44]. The model is based on an activation process, α, increasing from $\alpha = 0 \rightarrow 1$ during favourable condition for decay of wood, and decreasing $\alpha \rightarrow 0$ during non-

favourable conditions. The percentage of irreversible mass loss of wood, abbreviated "*ML*", increase when activation process α = 1.

The decay model was calculated based on a dataset with 60 min interpolated values of the original measurements. The model was started at an initial activation process of α = 0 in the three measurement points in the masonry wall, Point 1, 2 & 3.

3 Results

The results in this paper are experimental measurements obtained from a 2 year and 8 months monitoring period, together with inspections and on-site investigations. All raw and analysed measurement data from the experiment, have been provided in [71].

The following suffixes have been used to illustrate the different variations of data.

- "_Point=#", e.g. _Point=1, denote the measurement point, as described earlier in section 2.3.
- "_int" describe interpolated values. These interpolated values are calculated every 60 minutes, are used as input for calculation of mould index, *M*, activation process, α, and decay mass loss, *ML*.

The date x-axis is for all graphs formatted as: "month(year)".

3.1 Boundary conditions

The measured boundary conditions, relative humidity, *RH*, and temperature, Θ, in the two indoor rooms and three outdoor locations can be seen in Figure 5. Relative humidity is illustrated with solid lines, temperature with dashed lines. The 2 y-axes show the same range with the purpose to isolate the relative humidity and temperature data and increase the readability.

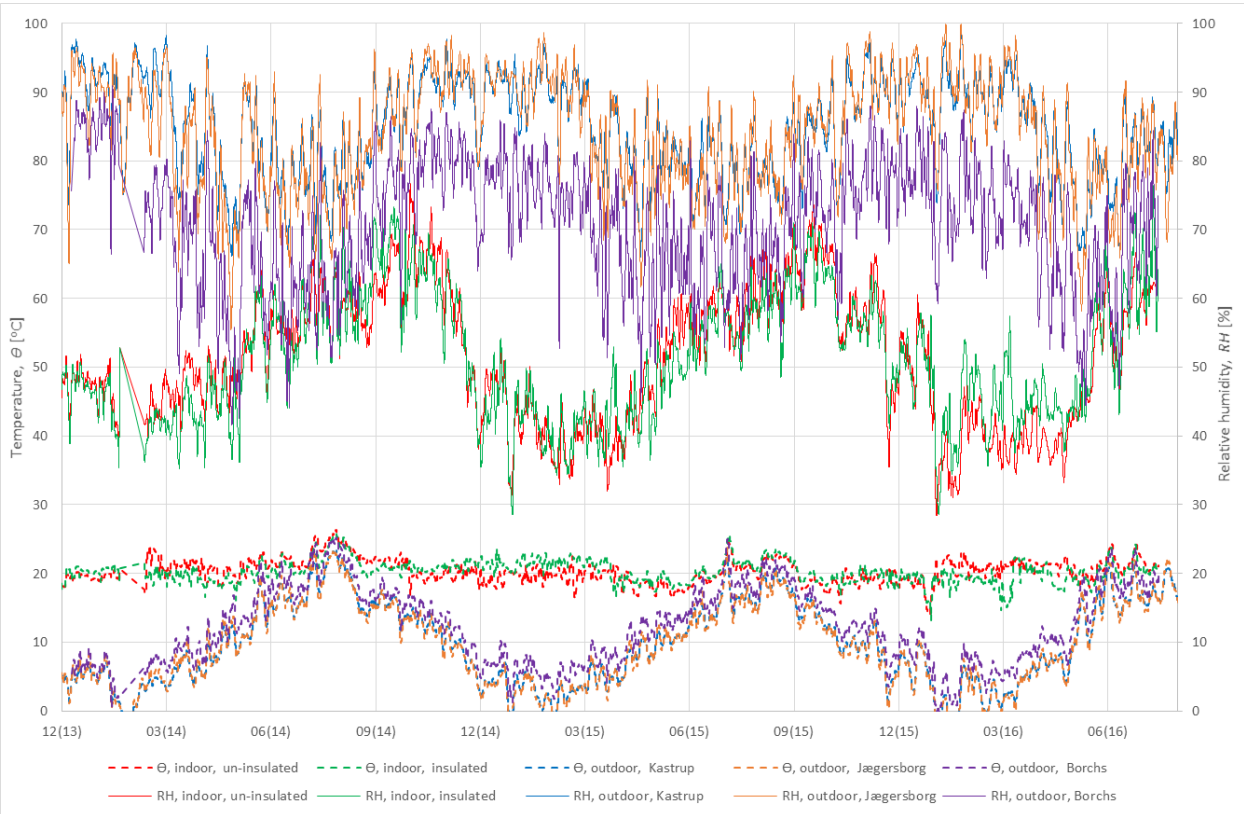

Figure 5 2-day averages of measured indoor and outdoor climate conditions.

3.2 Measurements in walls

The measured raw data with the T301.COW instrument, resistance, *R*, and temperature, Θ, have been calculated into relative humidity, *RH*, using the method described in Section 2.3.1. The values from the 4 sensor points in the insulated solid masonry spandrel can be seen in Figure 6. The values from the 3 sensor points in the un-insulated solid masonry spandrel can be seen in Figure 7. The location of the sensor points can be seen in Figure 2 and Figure 3. Relative humidity is illustrated with solid lines, temperature with dashed lines.

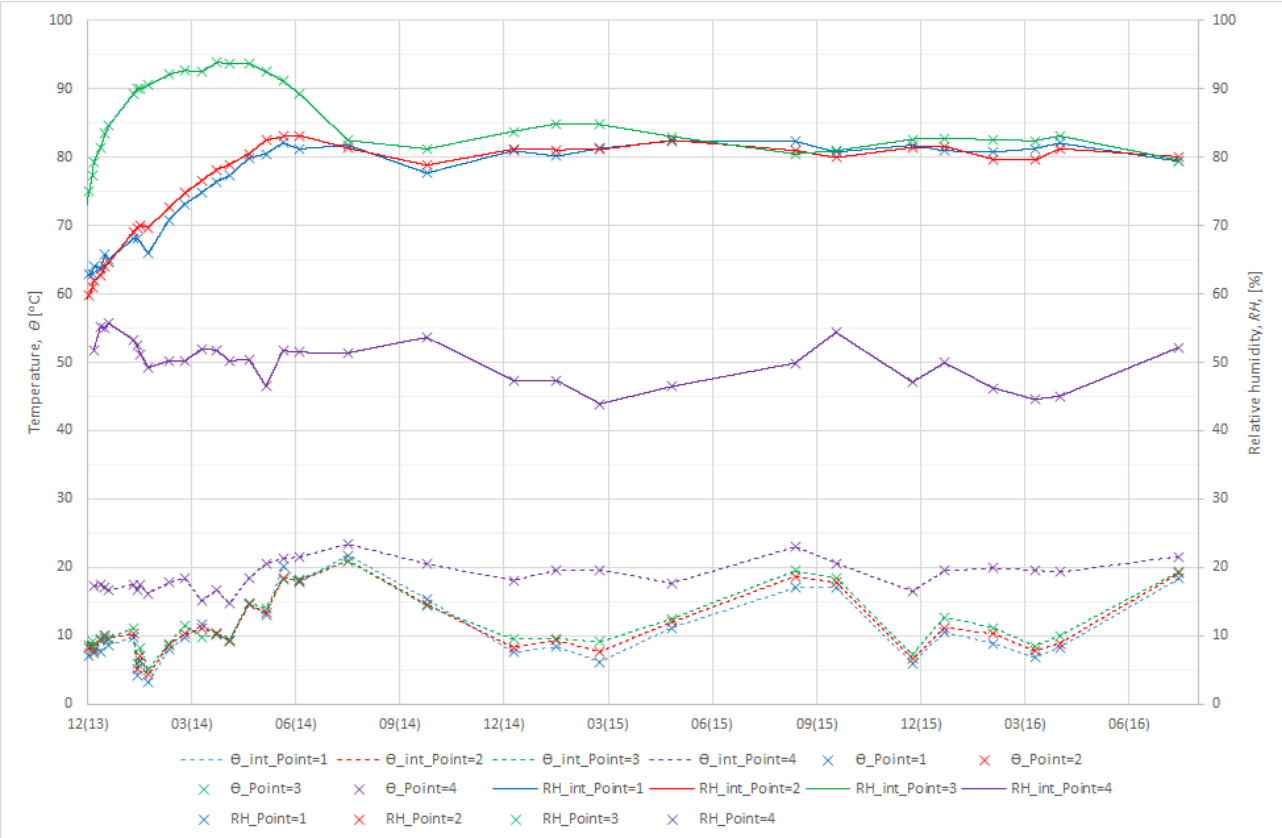

Figure 6 Measured temperature, Θ, and calculated relative humidity, RH, for insulated spandrel in Room 9

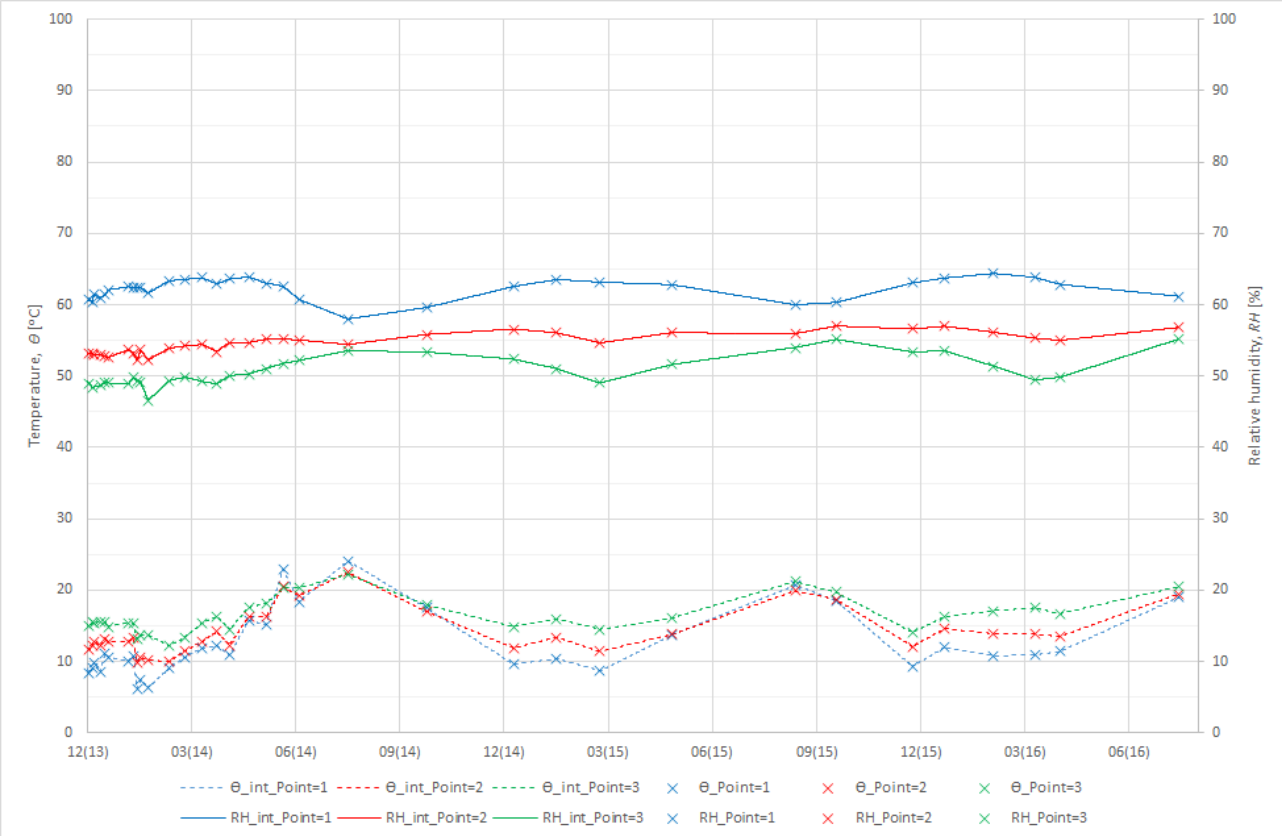

Figure 7 Measured temperature, Θ, and calculated relative humidity, RH, for un-insulated spandrel in Room 12

3.3 Thermal images of cold surfaces at start of project

An investigation of cold surface temperatures observed on the interior building envelope via thermographic pictures was performed before installing interior insulation. Thermographic pictures of the original spandrels in Room 9 and 12 can be seen in Figure 8 and Figure 9 respectively. A photograph of the measured area is inserted in the bottom left corner and a temperature scale is inserted on the right-hand side. The top left corner of Figure 9 show an additional thermographic picture of the spandrel in Room 12. The spot measurements (*Sp1 to Sp4*) in the figures indicate points where temperatures have been measured, with values given in the figure captions.

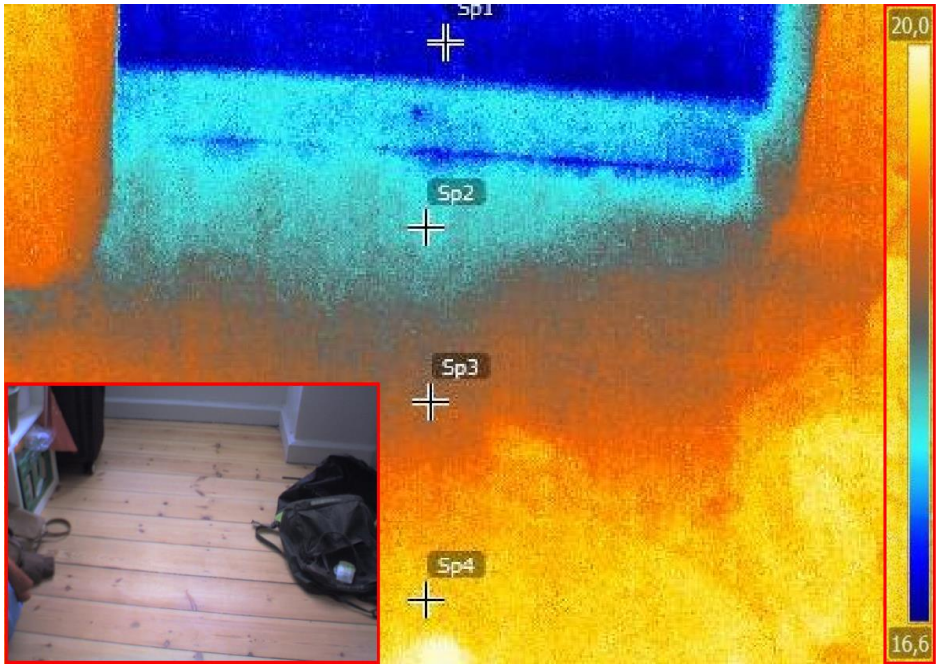

Figure 8 Thermal image in Room 9. Bottom left: Photograph. Θ_{Sp1} = 16.7 °C, Θ_{Sp2} = 17.8 °C, Θ_{Sp3} = 18.5 °C, Θ_{Sp4} = 19.5 °C. Outdoor temperature at time of investigation: Θ_{out} = 13.7 °C. Material by courtesy of ISOLINK & Erik Møller Arkitekter.

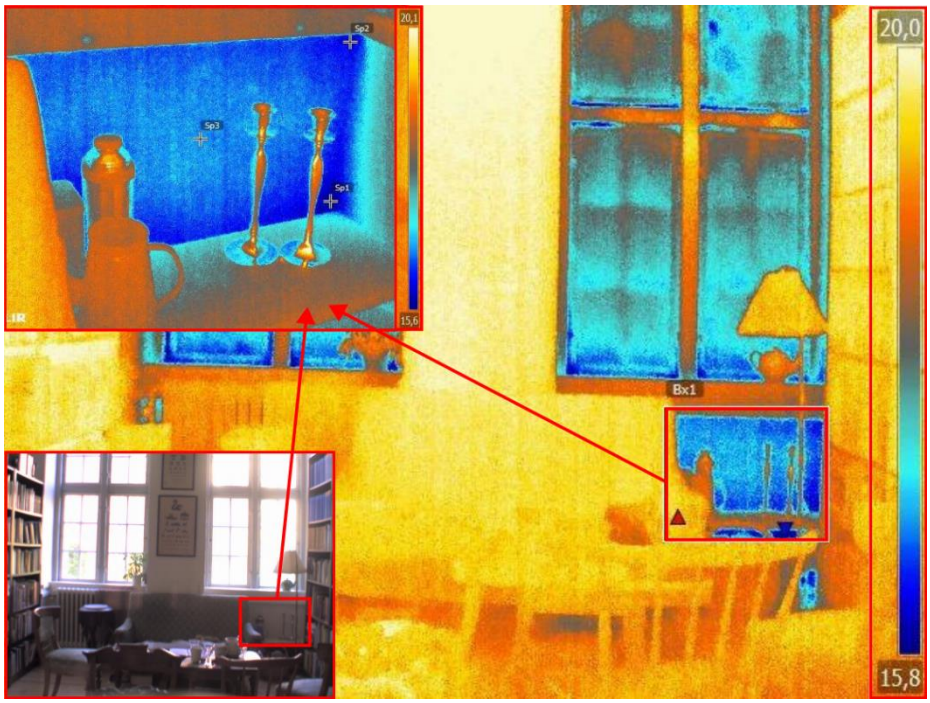

Figure 9 Thermal image in Room 12. Bottom left: Photograph. Top left: Thermal image of Bx1. Θ_{Sp1} = 15.6 °C, Θ_{Sp2} = 15.8 °C, Θ_{Sp3} = 16.7 °C. Outdoor temperature at time of investigation: Θ_{out} = 13.7 °C. Material by courtesy of ISOLINK & Erik Møller Arkitekter.

3.4 Visual inspection of frost damage to the exterior façade

The exterior façade of the insulated spandrel was visually inspected to determine if frost damage occurred during the experiment and up until 1 year after termination of the monitoring period. A photograph of the last visual inspection can be seen in Figure 10.

Figure 10 Last visual inspection of exterior surface of insulated spandrel on 2017-07-24.

3.5 Results from on-site investigation of mould via Mycometer®-test

Eight Mycometer tests were performed in the room with an insulated spandrel, 3 years and 8 months after installation of interior insulation. The tests consisted of five Mycometer-surface and three Mycometer-material tests. The results of the tests were reported as FLouresence Units (FLU) and a category defining presence of mould (spores), as described in Section 2.6.

The Mycometer-tests were performed after the procedure defined in the following numerated list, with results extracted from the laboratory report [72] as bullet points.

1. Test of interior surface, location: Between columns, 60 cm from floor.
    - Mycometer surface test resulting in FLU = 0 = Category A.
2. Test of interior surface, location: Next to P4, 6cm from floor.
    - Mycometer surface test resulting in FLU = 0 = Category A.
3. Test of interior surface, location: Other spandrel in same room, next to radiator.
    - Mycometer surface test resulting in FLU = 4 = Category A.
4. Clean ø105 mm Core-bit with alcohol: First in bath, then with freshly soaked paper towel. Drill core horizontally between columns, 60 cm from floor. Drilled through insulation system and original rendering, into original masonry wall.
    - Test of brick/mortar surface, behind original interior rendering.
        - Mycometer surface test resulting in FLU = 6 = Category A.
    - Material sample from extracted core, layer between original interior rendering and insulation adhesive.
        - Mycometer analysis of mould growth inside cement containing materials resulted in FLU = 18 = Category A.
    - Material sample from extracted core, joint between two insulation boards.
        - Mycometer analysis of mould growth inside cement containing materials resulted in FLU = 29 = Category A.
5. Clean ø105 mm Core-bit with alcohol: First in bath, then with freshly soaked paper towel. Drill core in P4, edge of Core-bit on floor. Drilled through insulation system, stopped with original interior rendering intact and insulation adhesive removed.
    - Test of original interior rendering surface.
        - Mycometer surface test resulting in FLU = 131 = Category B.
    - Material sample from extracted core, adhesive and insulation material.

- Mycometer analysis of mould growth inside cement containing materials resulted in FLU = 91 = Category B.

4 Discussion

The discussion is split into six parts in the following subsections, each dealing with a part of the results from the experiment. The sections include the boundary conditions of the experiment, evaluation of the monitored temperature and relative humidity at the 7 sensor points, evaluation of risk of damage based on frost, mould and decay of wood, and evaluation of cold surfaces.

The following suffix has been used to illustrate the different variations of data.

- "_decline=#", e.g. decline=0.05, refers to declination factors when calculating mould index, *M*, as described in Section 2.5.

4.1 Boundary conditions

To validate the measured outdoor values, a comparison between the data from the outdoor HOBO logger at Borchs dormitory and the weather stations in Kastrup and Jægersborg is shown in Figure 5. This comparison was initiated because unexpected low relative humidity and high temperature were measured locally at Borchs dormitory. The humidity by volume for each station were calculated and plotted in Figure 11. The comparison showed low difference between the three stations. The measured local outdoor conditions were assessed to be valid for calculating the excess humidity by volume from outdoor to indoor in the two rooms. These values were used to evaluate the moisture load in the rooms, based on humidity classes [13,57].

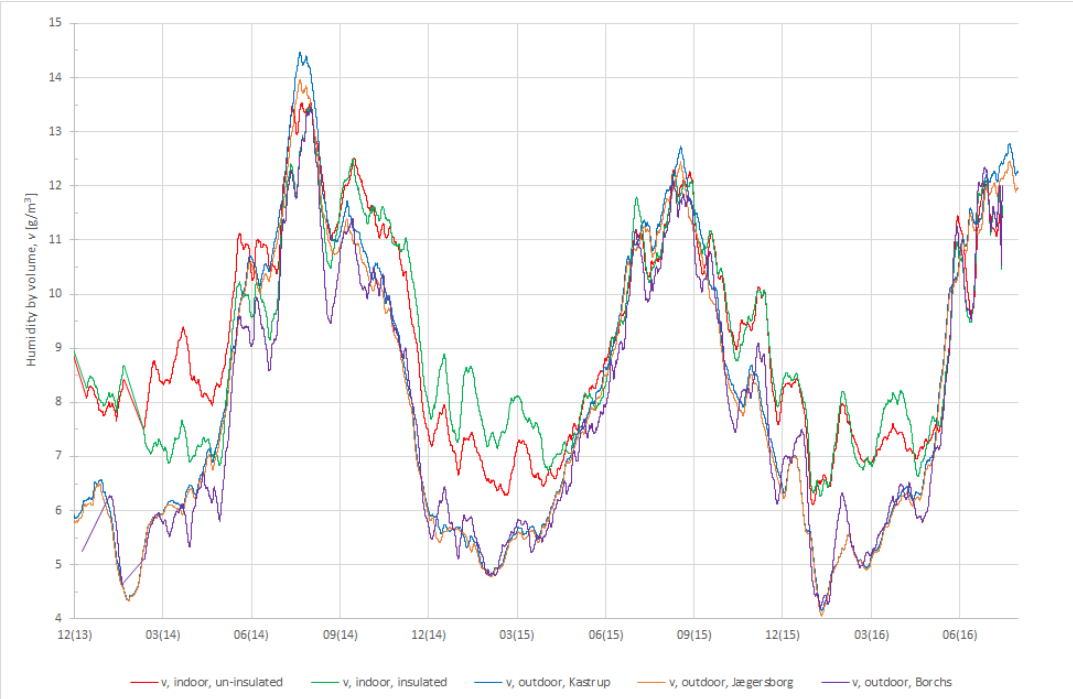

Figure 11 28-day average of calculated humidity by volume for the indoor and outdoor climates.

Differences between the humidity by volume in the two rooms appear from the beginning of 2014 until beginning of 2015, but with opposite sign in the two years. We found that this originated from the number of residents inhabiting the rooms. During the monitoring period, the residents in the rooms changed

several times. The period each resident(s) has lived in the room is marked with merged cells in Table 1, with text stating gender and age when moving in and out in brackets.

	2013	2014												2015												2016						
	Dec	Jan	Feb	Mar	Apr	May	Jun	Jul	Aug	Sep	Oct	Nov	Dec	Jan	Feb	Mar	Apr	May	Jun	Jul	Aug	Sep	Oct	Nov	Dec	Jan	Feb	Mar	Apr	May	Jun	Jul
Room 09: Insulated	Female (27-28)				Female (28-29)				Female (28-29) & Female (23)					Male (26-27)												Male (27-28)						
Room 12: Un-insulated	Male (27)			Male (27-28) & Female (29-30)					Male (26-28)																	Female (27)						

Table 1 Residents during experiment

The indoor humidity by volume of the two rooms, Figure 11, shows values following the outdoor climate, with a moisture excess to the indoor air caused by the occupant activity. The calculated monthly mean indoor excess of humidity by volume over the monthly mean outdoor temperature for both rooms can be seen in Figure 12. The results show that the room with an insulated spandrel has an excess of indoor humidity by volume in the coldest months lower than humidity class 2, following the slope of class 2. The room does not exceed humidity class 2, defined as *"Offices, dwellings with normal occupancy and ventilation"* [57].

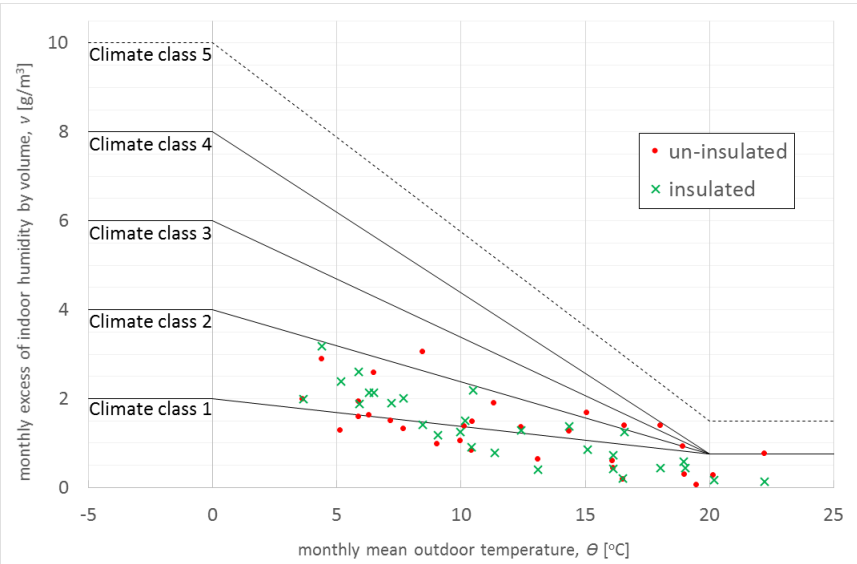

Figure 12 Excess of indoor humidity by volume in rooms, based on outdoor climate. Humidity classes from [13,57].

The values in Figure 12 show that the experimental conditions for the insulated room can be classified as being within the expected normal climate conditions for dwellings.

4.2 Measured temperature and relative humidity in masonry wall

The difference and magnitude of the measured hygrothermal conditions in the masonry part of the insulated and un-insulated wall have been compared. When comparing the insulation-induced change in temperature from Figure 7 to Figure 6, the main temperature drop takes place in the insulation layer, as expected. This results in notable lower temperatures throughout the masonry with a low difference from inside to outside. A similar change can be seen for relative humidity, with insulation resulting in high relative humidity throughout the wall and a low difference from inside to outside. The changed hygrothermal conditions are especially seen during the winter periods. E.g. in the second winter, the relative humidity and temperature at the time of measurement in the original un-insulated wall in Figure 7 lies within a band ranging from 63 % RH and 10 °C at the outside to 52 % RH and 15 °C at the inside of the masonry wall. The relative humidity and temperature measured at the same time in the insulated wall in Figure 6 lies within a narrow band ranging from 84 % RH and 8 °C on the outside to 86 % RH and 10 °C at the masonry wall towards the inside.

The generally changed humidity level induced by applying interior insulation to the walls can be seen by evaluating the average relative humidity in the period after initial dry-out (July, 2014) until the end of the monitoring experiment. The values for the Points 1/2/3 of the un-insulated wall show 62/56/52 % RH. The equivalent values for Points 1/2/3 in the insulated wall show uniformly distributed values of 81/81/82 % RH.

4.3 Evaluating risk of frost damage

As stated in the introduction, evaluation of frost damage is governed by 3 criteria occurring at the same time [30], of which two have been evaluated in this investigation: Temperature below freezing and wet masonry. As it can be seen in Figure 6, the interior insulated masonry wall becomes wetter than the un-insulated wall in Figure 7, but as the maximum measured relative humidity in the exterior masonry measurement Point 1 = 82% RH, we presume that the masonry does not reach a wet state (RH > 98 %) in the time between the manual measurements. The temperature conditions have been evaluated by plotting the raw data for locally measured temperature in the nearby bicycle shed in Figure 13. While the climate stations show periods with temperature down to -10 °C over some days in consecution (not shown in paper), the local temperatures only go below freezing 2 times during the 3 monitored winters, to a minimum temperature of -2 °C. The wall will have a significant contribution of heat from the inside, as only part of the wall is insulated. From this, we presume the temperature in the outer layer of the masonry do not drop below the freezing point in the time between the manual measurements.

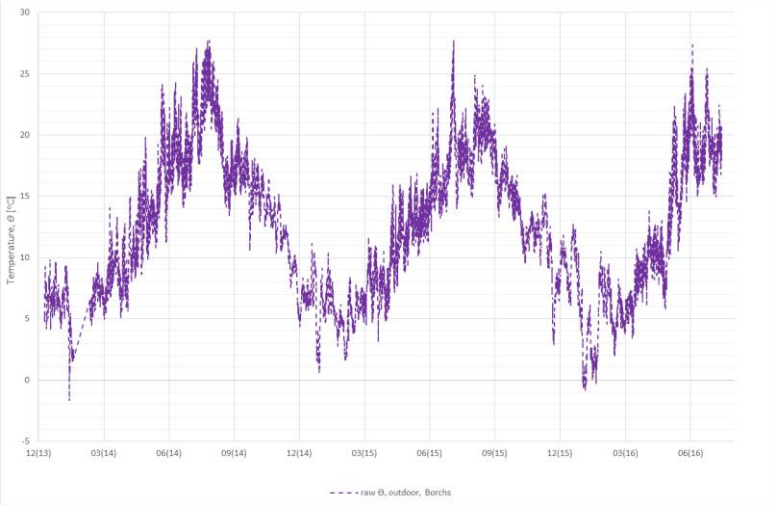

Figure 13 Measured outdoor temperature in nearby open bicycle shed

A final visual inspection was carried out one year after the termination of the monitoring experiment. As can be seen in Figure 10, no frost damage of the external wall was observed during the experiment.

4.4 Evaluating risk of mould: Mathematical and measured on-site

The VTT mould model [36] described in the Section 2.5, was applied to the measured values of Point 3 and 4 for the insulated wall presented in Figure 6 and Point 3 for un-insulated wall presented in Figure 7. The outcomes with mould index > 0 can be seen in Figure 14, with a maximum mould index of M=0.3 obtained at Point 3 for the insulated wall during the initial dry-out period. Using the evaluation scheme described in [37] for the interface layer, it becomes clear that even if the installed insulation system had not been based on cementitious material, then the calculated mould index would still have resulted in the category 0 < M < 2 = "acceptable". As the Xella Multipor insulation board were mounted with light mortar, which according to [73], contains more than 20 weight-% Portland cement, the glue can be categorized as a cementitious material. Ojanen et al. found that during construction with cementitious materials, the alkaline conditions

prohibit mould formation on new surfaces [37]. Based on this, a new starting point for mould growth was defined at the date of initial drying: 2014-07-17. The mould models with this new starting point did not show risk of mould growth. Evaluation of mould for the un-insulated wall indicated no risks of mould growth.

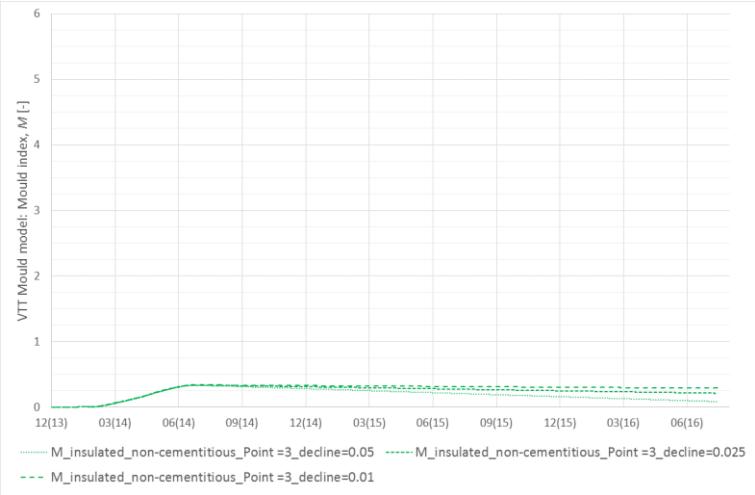

Figure 14 Results from calculated VTT mould and decay models > 0, based on values for insulated (Figure 6) and un-insulated (Figure 7) wall.

On-site investigation of mould growth of the insulated wall using Mycometer tests showed 6 of 8 samples within category A: below background level. The two samples taken behind the insulation in P4, close to the floor, had results within category B: above background level. Thereby, no physical mould growth was found on or behind the insulation board.

4.5 Evaluating risk of mass loss by decay of wood

It is important to emphasise that the traditional solid masonry spandrels did not contain wooden elements. Evaluation of risk of mass loss by decay of wood was based on the hypothesis that increase of moisture in the masonry could influence nearby wooden components. The wooden components being the wooden floor and the load bearing structure underneath. The added interior insulation to the masonry spandrel join the existing wooden floor, as can be seen in Figure 2. The load bearing structure of the historic multi-storey buildings consisted of wooden beams, holding the floor and supported by the solid masonry façade columns, or on a wooden exchange running parallel to the façade [5,6].

The model to calculate decay of wood described by Viitanen et al. [44] was applied to the measured values of the un-insulated wall in Figure 7 and the insulated wall in Figure 6. The model showed an activation process not exceeding 0 in the monitoring period at either of sensor Point 1, 2 or 3. As the activation process did not reach a value of 1, this indicates no calculated risk of decay of wood at either point in the solid masonry wall.

As the open floor structure experiences better hygrothermal conditions than the masonry/interior insulation interface, there appears to be no risk of decay of the wooden components. The better hygrothermal conditions derive from the natural ability of wood to distribute moisture along the fibres and evaporate excess moisture to the adjacent air, being the room air and the air volume on top of and below the traditional floor structure, compared to the closed masonry/insulation interface.

4.6 Cold surfaces

An investigation of thermal irregularities was performed in the beginning of the project, before interior insulation was installed at the spandrel of Room 9. The outdoor temperature was measured to be Θ_{out} = 13,7 °C at the time of the investigation. The temperatures recorded at the un-insulated surfaces of the spandrels were (Figure 8:Θ_{Sp1}) = 16.7 °C in Room 9 and (Figure 9:Θ_{Sp1}) = 15.6 °C in Room 12.

The floor temperatures were recorded by thermal imaging in Room 9, indicating low floor temperatures in front of the spandrel and into the building, with a measured floor temperature of (Figure 8:Θ_{Sp2}) = 17.8 °C in between the columns and (Figure 8:Θ_{Sp3}) = 18.5 °C approximately 0.5 meter from the spandrel. It is stated in [11] that an acceptable temperature range for bare feet/socks combined with pinewood floor of 18.5-31 °C for short term exposure and 22.5-28 °C for long term exposure, with an additional temperature increase in both cases of +1/2 °C for sedentary activity. Temperature ranges when wearing light shoes were treated in [12], stating an acceptable floor temperature range for indoor environment category A/B being 19 – 29 °C, and C being 17 – 31 °C. Based on the temperature ranges and monitored temperatures, the temperature in the case was on the limit of the lowest indoor class for occupants wearing light shoes. Putting the numbers in perspective: Traditional indoor footwear for Danish occupants are bare feet/socks, and the external design temperature is $\Theta_{out,design}$ = -12 °C [8].

It is evident that comfort can be improved for both asymmetric radiation and floor temperature by reducing the cold surface, such as by application of interior insulation. Such comfort improvement will increase the deviation from the limit for asymmetric radiation and act positively regarding the indoor environment class in respect to floor temperature. An example of the effect from applying interior insulation is illustrated by the increased surface temperature compared to the room air temperature seen in Figure 15. The values in Figure 15 include the values for the interior surface temperature, inside ambient air temperature and outdoor ambient air temperature at the time of manual measurements.

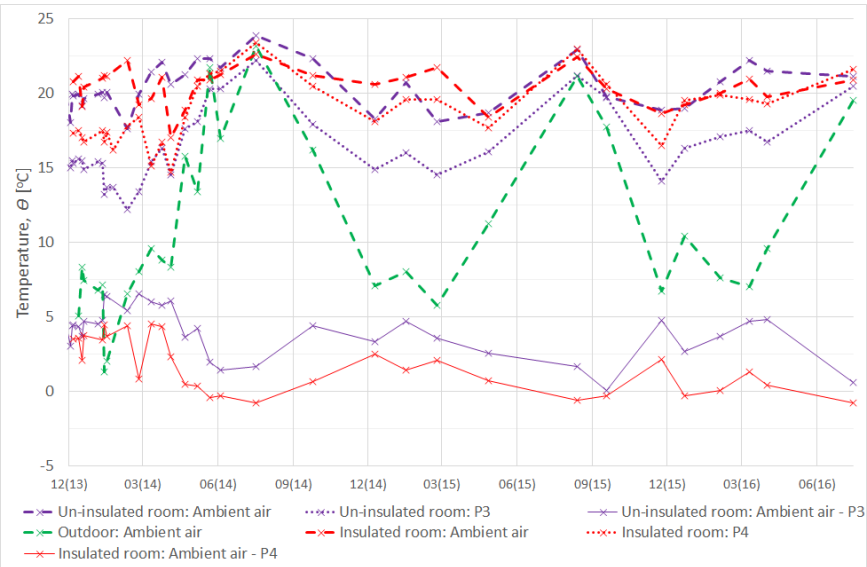

Figure 15 Ambient air temperature, interior surface temperatures and difference between the two at the time of manual measurements

Based on the temperature differences seen in Figure 15, it can be concluded that the surface temperature on the un-insulated spandrel was within the 10 °C limit for asymmetric radiation [9,10], but the deviation between surface and ambient air temperature decreased when interior insulation was applied.

5 Conclusion

This study has described an experimental investigation into the effect of installing interior insulation to the spandrels of a historic listed multi-storey dormitory building with solid masonry walls in the Danish capital, Copenhagen. Before the application, low interior surface temperatures of floors and façade walls were registered via thermal imaging. During the experiment, temperatures were monitored continuously on the inside of the un-insulated spandrel of a room that showed seasonally low surface temperatures and high difference between room air and surface temperature. Another room of the dormitory had an insulated spandrel, which had an increased surface temperature and a smaller difference between indoor air and surface temperatures.

The overall outcome of the results show that when applying interior insulation to the spandrel of a solid masonry wall subject to expected normal indoor climate, then the magnitude of relative humidity throughout the wall increases and temperature decreases, and there will be only small differences between inside and outside. The changed hygrothermal conditions have been evaluated visually for frost and mould, supplemented by on-site inspections for mould and mathematical predictions of risk of mould and decay of wood. Neither of the evaluated damage criteria showed damage after application of interior insulation.

It must be noted that conclusions in this paper are based on a healthy apartment with beneficial boundary conditions on the inside and outside, similar to a large segment of buildings in historic town centres [23]. The façade had a low impact of wind driven rain, combined with a rendered and painted façade. The temperature conditions in the courtyard were high, so the wall did not experience temperatures below freezing point. The indoor excess of humidity by volume in the room with an insulated spandrel did not go beyond humidity class 2 "*Offices, dwellings with normal occupancy and ventilation*" [13,57]. If the inside and outside boundary conditions get worse, then the risk of moisture induced damage, such as mould [20], decay of wood, and frost can increase.

6 Acknowledgements

Allan Ulrick Døi and Rasmus von Wurstemberger Nielsen for the initial work, conducted during their B.Sc. thesis [55].

Jan Ringgaard from J E R Byggeservice/BMT Instruments provided wooden dowels and helped with installation.

Xella Denmark for installation of Multipor system to the spandrel of Room 9.

This work was supported through the Danish industrial PhD program by Innovationsfonden [grant number 1355-00129]; COWIfonden [grant number C-123.01]; and COWI A/S.

7 References

[1] J. Kragh, K.B. Wittchen, Development of two Danish building typologies for residential buildings, Energy Build. 68 (2014) 79–86. doi:10.1016/j.enbuild.2013.04.028.

[2] K.B. Wittchen, J. Kragh, O.M. Jensen, Energy saving potentials – A case study on the Danish building stock, ECEEE 2011 SUMMER STUDY • ENERGY Effic. FIRST Found. A LOW-CARBON Soc. (2011) 1355–1363.

[3] M. Morelli, S. Svendsen, Investigation of interior post-insulated masonry walls with wooden beam ends, J. Build. Phys. 36 (2012) 265–293. doi:10.1177/1744259112447928.

[4] M. Morelli, L. Rønby, S.E. Mikkelsen, M.G. Minzari, T. Kildemoes, H.M. Tommerup, Energy retrofitting of a typical old Danish multi-family building to a “nearly-zero” energy building based on

experiences from a test apartment, Energy Build. 54 (2012) 395–406. doi:10.1016/j.enbuild.2012.07.046.

[5] J. Engelmark, Københavnsk etageboligbyggeri 1850-1900. En byggeteknisk undersøgelse, Statens Byggeforskningsinstitut, Hørsholm, 1983.

[6] J. Engelmark, Dansk Byggeskik : Etagebyggeriet gennem 150 år, 1. edition, Realdania Byg, 2013.

[7] G.R. Finken, S.P. Bjarløv, R.H. Peuhkuri, Effect of facade impregnation on feasibility of capillary active thermal internal insulation for a historic dormitory - A hygrothermal simulation study, Constr. Build. Mater. 113 (2016) 202–214. doi:10.1016/j.conbuildmat.2016.03.019.

[8] DS 418:2011, Beregning af bygningers varmetab/Calculation of heat loss from buildings, Charlottenlund, 2011.

[9] P.O. Fanger, H. Lund, H.E. Hansen, P.O. Danig, P. Kjerulf-Jensen, B. Elbæk, P. V. Nielsen, S. Aggerholm, F. Antvorskov, J. Gustavsson, O.B. Stampe, T. Lund Madsen, P.O. Danig, P. Worsøe-Schmidt, Danvak Grundbog i varme- og klimateknik, 3rd ed., Danvak APs, Vojens, Denmark, 2006.

[10] P.O. Fanger, B.M. Ipsern, G. Langkilde, B.W. Olesen, N.K. Christensen, S. Tanabe, Comfort Limits for Assymetric Thermal Radiation, Energy and Buildigns. 8 (1985) 225–236. doi:10.1016/0378-7788(85)90006-4.

[11] DS/ISO/TS 13732-2:2011, Ergonomics of the thermal environment – Methods for the assessment of human responses to contact with surfaces – Part 2: Human contact with surfaces at moderate temperature, 1. edition, Dansk Standard/Danish Standards, Charlottenlund, 2011.

[12] DS/EN ISO 7730:2006, Ergonomics of the thermal environment – Analytical determination and interpretation of thermal comfort using calculation of the PMV and PPD indices and local thermal comfort criteria, 2. edition, Dansk Standard/Danish Standards, Charlottenlund, 2006.

[13] E. Brandt, E.B. Møller, T. Bunch-Nielsen, G. Christensen, C. Gudum, M.H. Hansen, SBi Anvisning 224: Fugt i bygninger, 2.0, Statens Byggeforskningsinstitut, SBI, 2013.

[14] J. Munch-Andersen, SBi-anvisning 221 - Efterisolering af etageboliger, 1.0, Statens Byggeforskningsinstitut, SBI, Hørsholm, 2008.

[15] H.M. Kuenzel, Effect of interior and exterior insulation on the hygrothermal behaviour of exposed walls, Mater. Struct. 31 (1998) 99–103.

[16] G. Christensen, A.P. Kock, E.B. Møller, Indvendig efterisolering - ældre ydervægge af murværk, BYG-ERFA. (2015).

[17] Z. Pavlik, Hygrothermal performance study of an innovative interior thermal insulation system, Appl. Therm. Eng. 29 (2009) 1941–1946. doi:10.1016/j.applthermaleng.2008.09.013.

[18] G.A. Scheffler, Hygric performance of internal insulation with light-weight autoclaved aerated concrete, Proc. 5th Int. Conf. Autoclaved Aerated Concr. Sept. 15-16, 2011. (2011) 323–335. http://www.xella.com/de/docs/2011_Scheffler_InternalInsulation-LightWeightAAC-Multipor.pdf.

[19] J. Toman, A. Vimmrova, R. Cerny, Long-term on-site assessment of hygrothermal performance of interior thermal insulation system without water vapour barrier, Energy Build. 41 (2009) 51–55. doi:10.1016/j.enbuild.2008.07.007.

[20] J. Zhao, J. Grunewald, U. Ruisinger, S. Feng, Evaluation of capillary-active mineral insulation systems for interior retrofit solution, Build. Environ. 115 (2017) 215–227. doi:10.1016/j.buildenv.2017.01.004.

[21] M. Harrestrup, S. Svendsen, Full-scale test of an old heritage multi-storey building undergoing

energy retrofitting with focus on internal insulation and moisture, Build. Environ. 85 (2015) 123–133. doi:10.1016/j.buildenv.2014.12.005.

[22] A.A. Hamid, P. Wallent En, Hygrothermal assessment of internally added thermal insulation on external brick walls in Swedish multifamily buildings, Build. Environ. 123 (2017) 351–362. doi:10.1016/j.buildenv.2017.05.019.

[23] T. Odgaard, S.P. Bjarløv, C. Rode, Segment size, distribution, characteristics and 1d/2d/3d heat saving potential of multi-storey buildings with solid masonry walls in Denmark (Unpublished results/In press)., Energy Build. (n.d.).

[24] K. Ueno, J. Straube, R. Van Straaten, Field monitoring and simulation of a historic mass masonry building retrofitted with interior insulation, Therm. Perform. Exter. Envel. Whole Build. XII Int. Conf. (2013) 16.

[25] J. Straube, C. Schumacher, Interior Insulation Retrofits of Load-Bearing Masonry Walls in Cold Climates, J. Green Build. 2 (2007) 42–50. doi:10.3992/jgb.2.2.42.

[26] E. Vereecken, S. Roels, A comparison of the hygric performance of interior insulation systems: A hot box–cold box experiment, Energy Build. 80 (2014) 37–44. doi:10.1016/j.enbuild.2014.04.033.

[27] M. Saïd, Pe.R. Demers LL McSheffrey, Hygrothermal performance of a masonry wall retrofitted with interior insulation, Res. Build. Phys. (2003) 445–454. http://irc.nrc-cnrc.gc.ca/ircpubs.

[28] E. Vereecken, S. Roels, Capillary active interior insulation: do the advantages really offset potential disadvantages?, Mater. Struct. 48 (2015) 3009–3021. doi:10.1617/s11527-014-0373-9.

[29] T. De Mets, A. Tilmans, X. Loncour, Hygrothermal assessment of internal insulation systems of brick walls through numerical simulation and full-scale laboratory testing, in: 11th Nord. Symp. Build. Physics, NSB2017, Trondheim, Norway, 2017: pp. 11–14.

[30] M. Van Aarle, H. Schellen, J. Van Schijndel, Hygro thermal simulation to predict the risk of frost damage in masonry; effects of climate change, Energy Procedia. 78 (2015) 2536–2541. doi:10.1016/j.egypro.2015.11.268.

[31] H. Viitanen, J. Vinha, K. Salminen, T. Ojanen, R. Peuhkuri, L. Paajanen, K. Lahdesmaki, Moisture and Bio-deterioration Risk of Building Materials and Structures, J. Build. Phys. 33 (2010) 201–224. doi:10.1177/1744259109343511.

[32] K. Gradeci, N. Labonnote, J. Köhler, B. Time, Mould Models Applicable to Wood-Based Materials – A Generic Framework, in: 11th Nord. Symp. Build. Physics, NSB2017, 2017: pp. 11–14.

[33] E. Vereecken, S. Roels, Review of mould prediction models and their influence on mould risk evaluation, Build. Environ. 51 (2012) 296–310. doi:10.1016/j.buildenv.2011.11.003.

[34] K. Sedlbauer, Prediction of Mould Growth by Hygrothermal Calculation, J. Build. Phys. 25 (2002) 321–336. doi:10.1177/0075424202025004093.

[35] K. Sedlbauer, Prediction of mould fungus formation on the surface of and inside building components, Frauenhofer Institute, 2001.

[36] T. Ojanen, H. Viitanen, R. Peuhkuri, K. Lähdesmäki, J. Vinha, K. Salminen, Mold Growth Modeling of Building Structures Using Sensitivity Classes of Materials, Therm. Perform. Exter. Envel. Build. XI. (2010) 1–10. http://web.ornl.gov/sci/buildings/2012/2010 B11 papers/104_Ojanen.pdf.

[37] H. Viitanen, M. Krus, T. Ojanen, V. Eitner, D. Zirkelbach, Mold risk classification based on comparative evaluation of two established growth models, in: Energy Procedia, Elsevier B.V., 2015: pp. 1425–1430. doi:10.1016/j.egypro.2015.11.165.

[38] A. Hukka, H.A. Viitanen, A mathematical model of mould growth on wooden material, Wood Sci. Technol. 33 (1999) 475–485.

[39] A.M. Reeslev, M. Miller, Måling af skimmelsvampe i bygninger – hvorfor og hvordan?, Byggeindustriens Byggeforum. (2002) 18–19.

[40] M. Miller, M. Reeslev, Skimmelsporer og skimmelvækst er ikke det samme, Dansk Kemi. 1 (2003) 20–23. http://www.kemifokus.dk/skimmelsporer-og-skimmelvaekst-er-ikke-det-samme/.

[41] J.D. Krause, Analytical Instrument Performance Criteria Application: Application of a Fluorometric Method for the Detection of Mold in Indoor Environments, Appl. Occup. Environ. Hyg. 18 (2003) 1–5. doi:10.1080/10473220301457.

[42] M. Reeslev, M. Miller, The MycoMeter(TM)-Test: A new rapid method for detection and quantification of mold in buildings, Proc. Heal. Build. 1 (2000) 589–590.

[43] C. Brischke, S. Thelandersson, Modelling the outdoor performance of wood products - A review on existing approaches, Constr. Build. Mater. 66 (2014) 384–397. doi:10.1016/j.conbuildmat.2014.05.087.

[44] H. Viitanen, T. Toratti, · L Makkonen, R. Peuhkuri, T. Ojanen, · L Ruokolainen, J. Räisänen, Towards modelling of decay risk of wooden materials, Eur. J. Wood Prod. 68 (2010) 303–313. doi:10.1007/s00107-010-0450-x.

[45] G. Christensen, J. Kolbe, E. Brandt, Langtidsmåling af fugtforhold - i bygninger og bygningskonstruktioner, BYG-ERFA. (1999).

[46] E. Brandt, G. Christensen, M.H. Hansen, Fugtindhold i træ - måleudstyr, metoder og vurdering, BYG-ERFA. (1999).

[47] E. Brandt, M. Hjorslev Hansen, Fugtindhold i beton og murværk - måling og fejlkilder, BYG-ERFA. (2005).

[48] G. Christensen, Albertslund gårdhavehuse – opfølgende målinger i trætagkonstruktioner, TOR-NYT I/2001. (2001) 12–14.

[49] E. Brandt, Morten Hjorslev Hansen, O.H. Hansen, P. Mossing, Måling af træfugt ved modstandsmåling, Byggeindustrien. (1998) 26–30.

[50] E.J. de P. Hansen, Supplerende undersøgelser til SBI-rapport 268 - Byggematerialers frostbestandighed, Statens byggeforskningsinstitut (SBI), 1996.

[51] U. Lohse, SBI-Rapport 176: Laboratorieforsøg med fuger omkring trævinduer, Hørsholm, 1986.

[52] J.F. Munch-Petersen, Fugtmåledyvler, rapport nr. 198, Lyngby, 1990.

[53] K. Ueno, J. Straube, Laboratory Calibration and Field Results of Wood Resistance Humidity Sensors, in: Proc. BEST 1 Conf. June 10-12, Minneapolis, 2008.

[54] R. Walker, S. Pavía, M. Dalton, Measurement of moisture content in solid brick walls using timber dowel, Mater. Struct. 49 (2016) 2549–2561. doi:10.1617/s11527-015-0667-6.

[55] A.U. Døi, R. von W. Nielsen, Optimering af indeklimaforhold i fedede bygninger med fokus på ydervægskonstruktionen, The Technical University of Denmark, 2014.

[56] Agency for Culture and Palaces, Fredede & bevaringsværdige bygninger, Bygning: Collegium mediceum 1691, (1995). www.kulturarv.dk/fbb/bygningvis.pub?bygning=3180332 (accessed March 22, 2017).

[57] DS/EN ISO 13788:2013, Hygrothermal performance of building components and building elements

— Internal surface temperature to avoid critical surface humidity and interstitial condensation — Calculation methods, 2. edition, Dansk Standard/Danish Standards, Charlottenlund, 2013. http://www.iso.org/iso/catalogue_detail.htm?csnumber=51615.

[58] Bygge og Miljøteknik, Fugtmåler, T 301 COW, (2008) 2 pages.

[59] BMT Instruments ApS, COW T301, Vedbæk, 2017.

[60] Onset Computer Corporation, HOBO® U12-012 Logger, (2016) 2 pages. http://www.onsetcomp.com/files/data-sheet/Onset HOBO U12 Data Loggers.pdf.

[61] NCEI GIS Agile Team, National Oceanic and Atmospheric Administration (NOAA), National Centers for Environmental Information, Hourly/Sub-Hourly Observational Data Map, Version 1.8.2. (2017). https://gis.ncdc.noaa.gov/maps/ncei/cdo/hourly (accessed February 8, 2017).

[62] Bygge- og Miljøteknik, BM - Dybel: Elektrisk ledningsevne i afhængighed af fugtindhold, (n.d.) 1.

[63] K.K. Hansen, Technical report 162/86 Sorption Isotherms a Catalogue, Build. Mater. Lab. Tech. Univ. Denmark. 86 (1986).

[64] L. Ahlgren, Report 36: Fuktfixering i porösa byggnadsmaterial/Moisture fixation in porous building materials, Lund, Sweden, 1972.

[65] L. Due, Bygningsundersøgelseaf Borchs Kollegium, KBH. Sags. nr. 2682, Boeslunde, 2013.

[66] DS/EN 13187:1999, Thermal performance of buildings – Qualitative detection of thermal irregularities in building envelopes – Infrared method, DK-2920 Charlottenlund, 1999.

[67] mycometer, mycometer surface: On-site fungal contamination assessment, (2012) 2 pages. http://cdn.mycometer.com/fileadmin/user_upload/Pdf/Mycometer-Surface_Flyer__2012_.pdf.

[68] mycometer, Mycometer®: Instructions for surface sampling, (n.d.) 1. http://www.mycometer.com/products/mycometer-surface/surface-sampling/ (accessed July 25, 2017).

[69] Mycometer, Interpretation criteria for Mycometer results, (n.d.). http://www.mycometer.com/products/mycometer-surface/interpretation-criteria/ (accessed July 25, 2017).

[70] M. Schrock, C. Riffle, A. Dindal, J. Mckernan, J. Enriquez, Environmental Technology Verification Report: Mycometer ®-test Rapid Fungi Detection and Bactiquant ®-test Rapid Bacteria Detection Technologies, 2011.

[dataset] [71] T. Odgaard, S.P. Bjarløv, C. Rode, Measured and analyzed data from Borchs dormitory, (2017).

[72] S.A. Elborne, Hussvamp laboratoriet ApS, Mikrobiologisk analyse, case: 26996-1, Borchs kollegie, Birkerød, 2017.

[73] Fels-Werke GMBH, Product safety data sheet for Light mortar. Int. ref.: SDS_LM_X_e1073, Goslar, 2013.